RESEARCH ARTICLE

VOLCANICA

Magma residence time, ascent rate and eruptive style of the November ash-laden activity during the 2021 Tajogaite eruption (La Palma, Spain)

Barbara Bonechi*[α], Margherita Polacci[α], Fabio Arzilli[β], Jorge E. Romero[γ], Jonathan Fellowes[α], and Mike Burton[α]

[α] Department of Earth and Environmental Sciences, University of Manchester, Manchester, United Kingdom.
[β] School of Science and Technology, Geology Division, Camerino, Italy.
[γ] Instituto de Ciencias de la Ingeniería, Universidad de O'Higgins, Rancagua, Chile.

Abstract

We combined compositional analyses, crystal size distributions and geothermobarometry of tephra erupted during the 2021 Tajogaite eruption (La Palma, Spain), focusing on samples collected in November 2021 associated with a period of abundant ash emission characteristic of the second half of the eruption (from October onwards). Magma erupted in November exhibits a more primitive basanitic composition than the earlier magma. Crystallisation temperatures range between ~1100–1160 °C (H_2O = 1–3 wt.%) for phenocrysts and microphenocrysts, with corresponding pressures indicating depths from ~10 to ~30 km. Crystal size distribution analysis reveals short (minutes) residence times for plagioclase. Finally, magma ascent velocities (~0.01–0.3 m s^{-1}) suggest acceleration and fragmentation in the shallowest part of the conduit. Our results suggest that the trigger of the November explosive activity can be attributed to complex feedback between gas emission rates, changes in conduit geometry, and magma ascent rate.

Resumen

En este trabajo, combinamos análisis composicionales, distribuciones de tamaño de cristales y geotermobarometría de tefra de la erupción del volcán Tajogaite en 2021 (La Palma, España), centrándonos en muestras recogidas en noviembre de 2021 asociadas a un periodo de abundante emisión de cenizas, característico de la segunda mitad de la erupción (a partir de octubre). El magma emitido en noviembre exhibe una composición basanítica más primitiva que el magma inicial de la erupción. Las temperaturas de cristalización oscilan entre ~1100–1160 °C (H_2O = 1–3 peso %) para fenocristales y microfenocristales, con presiones que indican profundidades de ~10 a ~30 km. El análisis de la distribución del tamaño de los cristales revela tiempos de residencia cortos (minutos) para la plagioclasa. Por último, las velocidades de ascenso del magma (~0,01–0,3 m s^{-1}) sugieren aceleración y fragmentación en la parte somera del conducto. Nuestros resultados sugieren que la actividad explosiva observada en noviembre puede atribuirse a una compleja retroalimentación entre las tasas de emisión de gases, los cambios en la geometría del conducto y la velocidad de ascenso del magma.

Keywords: Pre-eruptive conditions; Basanitic melt; Crystal size distribution; Geothermobarometry; Ash-rich jets; Eruptive style.

Submitted: 2023-07-12 | Accepted: 2023-12-19 | Published: 2024-01-31

Editor: A. Whittington | Typesetter: J. Farquharson

1 Introduction

The magnitude and frequency of volcanic eruptions typically depend on both mechanisms and timescales of magma evolution during storage in crustal reservoirs and ascent in the volcanic conduit [Cassidy et al. 2018; Pappalardo and Buono 2021]. The study of petrological (textural and geochemical) features of natural volcanic rocks, combined with estimation of intensive variables (e.g. temperature, pressure) recorded by crystals at equilibrium, represents a powerful tool to obtain information about depth and physico-chemical conditions of volcano magma supply systems during storage and prior to eruption [e.g. Pioli et al. 2014; Pompilio et al. 2017; Gurioli et al. 2018; Thivet et al. 2020]. These parameters are also crucial for eruption forecast, hazard assessment and risk mitigation in areas of active volcanoes [Hammer et al. 1999; Blundy and Cashman 2008; Pappalardo and Buono 2021]. Moreover, in several studies focused on products of recent well-monitored eruptions, a systematic correlation between the petrology of erupted rocks and the pre- and syn-eruptive geophysical signals has been observed [e.g. Hammer et al. 1999; Cashman and McConnell 2005; Saunders et al. 2012; Pappalardo et al. 2014; Preece et al. 2016; Pappalardo and Buono 2021]. In this respect, the 2021 eruption of Cumbre Vieja (La Palma, Canary Islands) represents an opportunity to track conditions in the magmatic plumbing system by integrating a series of techniques (e.g. petrological, geochemical, geophysical, etc.) thanks to the availability of syn-eruptive open-source seismic and ground deformation data and observations from near-real-time field sampling campaigns [Dayton et al. 2023]. The newly formed eruptive centre, named Tajogaite, erupted from 19 September to 13 December 2021, producing the most significant recent historical eruption in the Canary Islands in terms of volume (~0.2 km^3 [Day et al. 2022]) and duration (85 days [Day et al. 2022]). The eruption has been described as hybrid [Bonadonna et al. 2022] because of the simultaneous occurrence of lava flows and tephra from multiple vents mostly associated with a variety of eruptive styles (e.g. lava flows, ash emissions, lava fountains, Strombolian activity), often alternating at different vents as well as at the same vent [Longpré and Felpeto 2021; Bonadonna et al. 2022; Pankhurst et al. 2022; Romero et al. 2022; Taddeucci et al. 2023]. Col-

* barbara.bonechi@manchester.ac.uk

Figure 1: Chronology of the eruptive activity during 13–18 November. [A] Continuous degassing (with minor ash content) on 13 November; [B] pulses of convective ash formed a 0.6–0.8 km high eruptive column which dispersed to form an umbrella cloud, and fountaining jet on the left of the ash cloud; [C] ash-loaded column on 14 November with gas-rich plume in the foreground; [D] single convective ash-laden column on 15 November; [E] continuous degassing on 16 November; [F] diffuse degassing associated with an ash-rich plume in the background on 17 November; [G] 50–80 m high lava fountain on 17 November associated with strong magma fragmentation leading to an ash-rich plume, in contrast to the one observed in [H] in the background; [H] vertical convective ash column producing brown ash emission, and the southeast vent sourced discontinuous fountaining events on 18 November.

lected lava and tephra samples throughout the eruption show temporal changes in mineralogy and bulk rock geochemistry from tephrite to basanite [Bonadonna et al. 2022; Carracedo et al. 2022; Day et al. 2022; Pankhurst et al. 2022; Romero et al. 2022; Dayton et al. 2023; Ubide et al. 2023]. As reported by Day et al. [2022], this temporal variation reveals that the beginning of the eruption was fed by a fractionated tephritic magma, followed later by deeper-sourced and more primitive magmas. Based on isotopic data and seismic precursors [Day et al. 2022], the initial fractionated tephritic magma was likely stored in the upper lithosphere (10–25 km depth) up to four years prior to eruption, while the later lavas and tephra were fed by more primitive basanitic parental magmas, showing a magmatic trend similar to that documented during the 1949 and 1971 Cumbre Vieja eruptions [Klügel et al. 2000; Barker et al. 2015].

Here, we combined compositional analyses, crystal size distributions (CSDs) data and geothermobarometry to quantify magma storage depth, pre-eruptive conditions and magma ascent timescales during the 2021 Tajogaite eruption. We par-

ticularly focused on a sample suite collected between 15 and 18 November 2021 which is related to a period of abundant ash emission followed by a return to typical eruptive activity (e.g. ash venting, lava fountaining, Strombolian activity, gas emissions etc.) during the following days (16–18 November). Hence, this eruption period represents an ideal case study to investigate the processes and physicochemical conditions in the plumbing system that may have led to observed changes in eruptive activity.

1.1 Tajogaite eruption from 13 to 18 November 2021

La Palma is the most historically active island among the Canary Islands, and the Cumbre Vieja ridge has fed eruptions in 1585, 1646, 1677–1678, 1712, 1949, 1971 [Carracedo et al. 1998; Guillou et al. 1998; Klügel et al. 2000; Carracedo et al. 2001; Casillas Ruiz et al. 2020]. The Tajogaite eruption in the Cumbre Vieja ridge began on 19 September 2021 after intense seismic unrest, geochemical anomalies, and deformation that started in 2017 [e.g. Carracedo et al. 2022; D'Auria et al. 2022; Pankhurst et al. 2022; Romero et al. 2022]. Here, we report a description of the activity occurred during the week 13–18 November 2021, during which we deployed a field campaign, observed the eruptive activity and collected the sample suite used in this study. On 13 November, the activity consisted of continuous degassing (with minor ash content) from the northwest summit vent (Figure 1A), while the southeast summit vent emitted pulsing jets of lava (100–150 m high) every 30–40 s. The activity of the northwest summit crater changed after 20.23 LT (Local Time), when pulses of convective ash formed a 0.6–0.8 km high eruptive column which spread laterally towards the southwest to form an umbrella cloud (Figure 1B). After midnight the summit activity decreased, and only weak Strombolian explosions (up to 50 m high) and continuous degassing was observed. During these events, lava effusion continued uninterrupted from the mid-northwest flank of the volcano. On 14 November, the morning activity consisted of a continuous jet of ash from the southeast vent, forming a vertical column ~1 km high and then being dispersed towards the west-southwest. During the afternoon, the southeast summit vent plume became ash-loaded, with a characteristic brown-to-grey colour, maintaining the same dispersal (Figure 1C). On 15 November morning, the ash-rich plume from the southeast vent changed direction towards the north-northwest, and its height reached 1–1.5 km. Medium-to-coarse ash (0.25–1.0 mm) was continuously falling at a distance of 8 km northwest from the main vents, while at Villa José (c. 13 km northwest) the plume deposited a continuous blanket of fine ash. The sustained explosive activity then transitioned to a pulsing behaviour, and, between 14.00 and 19.30 LT, continuous ash emission resumed at all the main vents, forming a single convective ash-rich column (Figure 1D) with intense lightning. On 16 November morning, the ash emission decreased considerably, and continuous degassing was present (Figure 1E). While the explosive activity was not visible or very weak during the night, a lava overflow occurred on 17 November at 02.01 LT, producing a large overflow event towards the west. In the morning, the activity consisted of shortly spaced (<1 minute) convective ash jets from the northwest summit vent, with dispersal towards the west, resulting into a weak plume less than 0.6 km high (Figure 1F). The explosive activity ceased completely around 16.30 LT and degassing persisted. The lull in activity persisted until 19.01 LT when it resumed producing an ash-laden weak convective column, which after 21 minutes also produced a 50–80 m high lava fountain (Figure 1G). The activity was variable on 18 November. In the afternoon, at 16.40 LT there was a vertical convective ash column that produced brown ash emission from the northwest vent, while the southeast vent sourced discontinuous fountaining events (Figure 1H).

2 Methods and materials

2.1 Analytical methods

Polished thin sections were produced for two samples of 15 November 2021 representative of the night (15_N) and morning (15_M) activity. Tephra particles of 15_N (fine lapilli) and 15_M (coarse ash) samples range in size (i.e. intermediate lengths of the particles) from 2 to 15 mm and from 0.5 to 1 mm, respectively. Two further sections were produced for samples of 17 (17 Nov) and 18 (18 Nov) November 2021 representative of the ash fall (<0.05 mm) deposited in those days. All these samples belong to tephra MU6.5 reported by Bonadonna et al. [2022] and Romero et al. [2022], which is characterised by an alternation of moderately to poorly sorted, grey to black coarse to fine ash. We would like to highlight that for our analytical measurements, we selected sample grain sizes for which post fragmentation processes are assumed to be not significant and for which sample texture and chemistry are considered representative of magma at the fragmentation level. Thin sections were carbon-coated and analysed with an FEI Quanta 650 FEG-SEM electron microscope (Department of Earth and Environmental Sciences, University of Manchester, UK) operated at 10 to 15 kV (for ash grains and polished thin sections, respectively) accelerating voltage, and a working distance of 10 mm. Chemical compositions of glass and crystals were obtained with a JEOL JXA-8530F field emission electron microprobe at the Photon Science Institute, University of Manchester, UK. The operating conditions were as follows: 15 kV accelerating voltage, 10 nA beam current, and beam spot diameter of 1 or 5 µm. Na was measured first to minimise volatilisation error and corrected for drift over time using time dependent intensity (TDI). Calibration standards were jadeite for Na and Al, forsterite for Mg, anorthite for Si, fayalite for Fe, tephroite for Mn, apatite for P, orthoclase for K, wollastonite for Ca and rutile for Ti. Analytical precision was between 1 and 5 % for major elements and up to 10 % for elements at concentration of < 0.2 wt.%. Analyses of clinopyroxenes, used for thermobarometry calculations, had 1 sigma relative error for Na between 3–7 %. Count times and calibration materials, alongside estimates of precision and accuracy are shown in Supplementary Material 2 Table S1.

2.2 Image processing

Textural analyses of the samples were performed on BSE images using the software `ImageJ v.1.54` [Abràmoff et al. 2004; Schneider et al. 2012]. In order to segment mineral phases and

vesicles, BSE images were converted into binary images by using the `Threshold` function based on the grayscale histogram of the image (Supplementary Material 1). Subsequently, the `Analyse Particles` function was used to calculate the following parameters: coordinates (X and Y), area (mm^2), orientation, roundness (0–1), and major and minor axis length (mm). We measured 2293 and 1309 plagioclases for sample 15_N and 15_M, respectively (Supplementary Material 2 Table S2).

Data were exported as `Microsoft Excel` worksheets (.xls; Supplementary Material 2), as well as using the CSD output plugin to save data as .csd files for use in `CSDcorrections v1.61` [Higgins 2000]. Image data quality was ensured throughout the data handling process by repeating exactly the same steps for each of the samples analysed.

Crystal fraction Φ_c of each phase was calculated on a vesicle-free basis by dividing the area of the crystal phase by the reference area used for the image analysis of natural samples.

Total areal vesicle number densities (VNDs) were calculated for both 15_N (fine lapilli) and 15_M (coarse ash) samples by dividing the number of vesicles by the total area and then transformed in 3D by dividing the value by the average vesicle equivalent diameter [Polacci et al. 2006]. We obtained VND average values of $5.1 \times 10^{12} \pm 3.3 \times 10^{12}$ m^{-3} for sample 15_N and $8.4 \times 10^{12} \pm 4.4 \times 10^{12}$ m^{-3} for sample 15_M (Supplementary Material 2 Table S2 and Supplementary Data).

2.3 CSD calculation

A limitation of grain sizes measured in thin sections is that the data represent 2D apparent crystal dimensions rather than 3D crystal shapes. To address this, the program `CSDcorrections` [Higgins 2000] was used to convert 2D intersection data to true 3D crystal size distributions by incorporating corrections for the intersection probability effect and cut-section effect. The first step in the conversion process is to estimate the 3D habit of the crystals within the sample, which were calculated using the `Microsoft Excel` macro `CSDslice` [Morgan and Jerram 2006]. `CSDslice` compares measured 2D minor and major crystal axis length data from `ImageJ` with a database of 2D crystal shapes. Using a linear regression, `CSDslice` provides a list of the top five best-fit estimates of the ratios between the short (x), intermediate (y) and long (z) crystal dimensions, based on the 2D input data. Each crystal habit ratio is also given an R^2 value, a statistical measure of how close the 2D data lie to the fitted regression line. According to Morgan and Jerram [2006], 3D crystal habits are well reproduced for $R^2 > 0.8$. Crystal habit estimates from `CSDslice` were inserted into `CSDcorrections` to calculate CSDs, together with measured area (mm^2), roundness (0–1) and crystal lengths (mm). Resulting CSD plots show the natural logarithm of the population density (mm^{-4}) against corrected crystal length (mm).

2.4 Componentry analysis

For the ash fall samples (< 0.05 mm) of 17 and 18 November 2021 componentry analysis was performed on polished thin sections with SEM imaging, following the protocol of Ross et al. [2022]. Basic componentry based on SEM images was performed by using the software `JMicroVision` Roduit [2007]* on image mosaics. We used the "manual point counting" feature of `JMicroVision` that allowed us to count all grains (Supplementary Material 1 Figures S1–S2). We analysed the proportion of different particles (crystals, glass, sideromelane and tachylite) considering between 400 and 600 points. `JMicroVision` files with the componentry analysis are available in Bonechi [2023].

2.5 Thermobarometry

Pre-eruptive pressures and temperatures from clinopyroxene-melt equilibria were calculated by using the open-source `Python3` package `Thermobar v. 1.0.26` [Wieser et al. 2022]. All `Thermobar Jupyter` notebooks and spreadsheets are available in Bonechi [2023]. Particularly, we used the `Cpx-Liquid Melt Matching` algorithm available in `Thermobar` [Wieser et al. 2022] to (i) pair our clinopyroxene compositions (Clinopyroxene.xlsx) with liquid compositions (Liquid_LaPalma2021.xlsx) from this study and from other literature data available for the entire La Palma 2021 eruption [Castro and Feisel 2022; Day et al. 2022; Pankhurst et al. 2022; Romero et al. 2022; Dayton et al. 2023; Ubide et al. 2023], and (ii) estimate pressure and temperature conditions. In order to obtain reliable pressure and temperature (P-T) estimations, we run the calculations for multiple different existing models: the barometer (SEE = ±1.4 kbar) of Neave and Putirka [2017] and the thermometer (eq. 33, SEE = ±45 °C) of Putirka [2008] (model MM_N17P08 in Bonechi [2023]); the barometer (SEE = ± 1.15 kbar) and thermometer (SEE = ±31.6 °C) of Masotta et al. [2013] (model MM_M13 in Bonechi [2023]); the barometer (SEE = ±5.0 kbar) and thermometer (SEE = ±23.8 K) of Putirka et al. [2003] (model MM_P03 in Bonechi [2023]); the barometer (SEE = ±5.0 kbar) of Putirka et al. [2003] and the thermometer (eq. 33) of Putirka [2008] (model MM_P03P08 in Bonechi [2023]); the barometer (eq. 30, SEE = ±1.6 kbar) and thermometer (eq. 33) of Putirka [2008] (model MM_P08 in Bonechi [2023]); and the barometer (eq. P2, SEE = ±1.51 kbar) and thermometer (eq. T2, SEE = ±23.8 K) of Putirka et al. [1996] (model MM_P96 in Bonechi [2023]). These combinations were chosen because they are the most appropriate for alkali magma compositions of La Palma magmas (e.g. MM_P03), they are commonly applied to mafic alkaline magmas (e.g. MM_P0308), and appropriate for liquids spanning from basalt to rhyolite, from picrite to phonolite, from tephrite to trachyte, and everything in between (e.g. MM_P08, MM_P96). We also widen the comparison by considering other combinations calibrated for tholeiitic composition (e.g. MM_N17P08) and alkaline differentiated magmas (e.g. MM_M13). To test for clinopyroxene-melt equilibrium we considered the equilibrium filters for DiHd, CaTs and EnFs errors (2 sigma values) from Neave et al. [2019], the $K_D = 0.27 \pm 0.03$ following Scruggs and Putirka [2018], and the K_D model of Masotta et al. [2013]. For P-T estimates we used only clinopyroxene-liquid pairs that passed the applied equilibrium tests, obtaining consistent temperature and pressure results among the considered models (Supplementary Material 2 Table S3 and Figure S3). For all these calculations to assess the effect of water content on P-T estimates,

*https://jmicrovision.github.io/

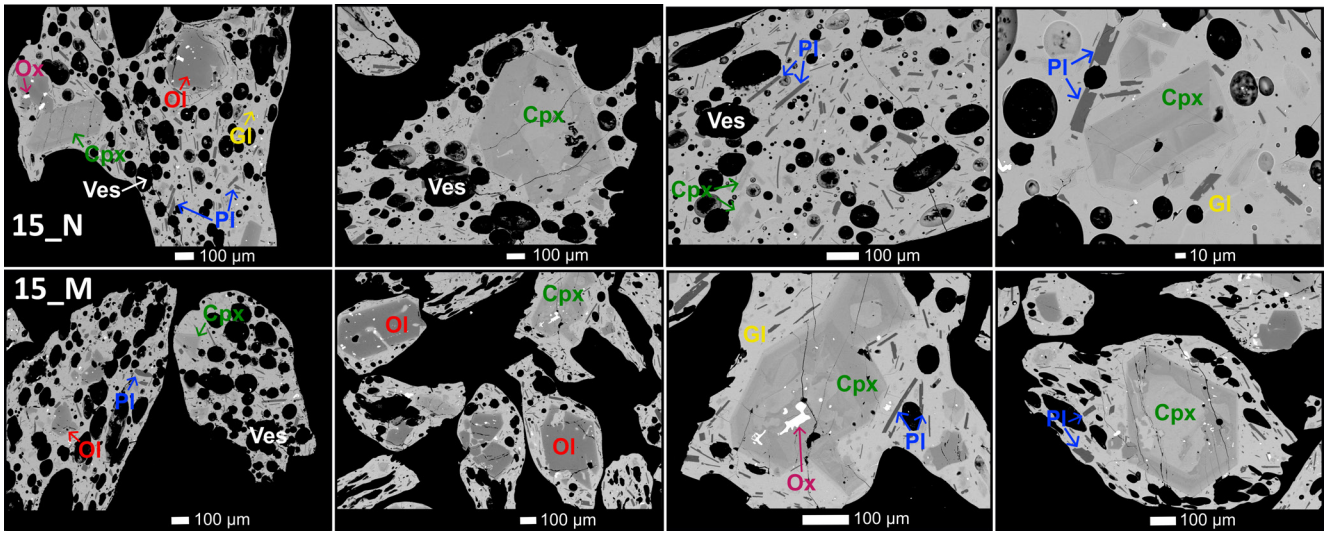

Figure 2: Backscattered images of samples from 15 November night (15_N) and morning (15_M). Cpx: clinopyroxene; Ol: olivine; Pl: plagioclase; Ox: oxide; Gl: glass; Ves: vesicle.

we considered water content ranging from 1 to 3 wt.% appropriate for the 2021 Tajogaite eruption [e.g. Burton et al. 2023; Fabbrizio et al. 2023; Ubide et al. 2023]. Caution is required for clinopyroxene-melt data because the thermobarometers have not been calibrated for highly alkaline systems like basanites and tephrites, potentially resulting in pressure overestimation (200–400 MPa [Putirka 2008; Dayton et al. 2023]). To address this, we plotted our data against the calibration dataset of different Cpx-based thermobarometers available on `Thermobar` [Putirka 2008; Masotta et al. 2013; Neave and Putirka 2017; Petrelli et al. 2020]. The results are available in Supplementary Material 1 Figures S4A–C and in Bonechi [2023]. Our data match well with the calibration dataset of Putirka [2008], Neave and Putirka [2017], and Petrelli et al. [2020], suggesting that the P-T estimates obtained in this study are reliable. Conversely, our data do not agree with the calibration dataset of Masotta et al. [2013], probably because their thermobarometry has been calibrated for alkaline differentiated compositions (e.g. trachytes and phonolites).

Pressures were converted to depths according to the crust and mantle densities of 2800 and 3111 kg m^{-3}, respectively [Ranero et al. 1995; Tenzer et al. 2013]. The transition between densities was determined based on the Moho position estimated at ~10 km depth [D'Auria et al. 2022].

3 Results

3.1 Mineralogy and textural features of selected samples

Sample clasts from 15 November 2021 are characterised by a vesicle fraction (Φ_v) ranging from 0.5 to 0.6. Vesicles are subrounded or rounded, with minor exceptions where vesicles are elongated and deformed around phenocrysts, and their size (i.e. maximum length) varies from 0.03 to 1.5 mm; vesicle coalescence is negligible (Figure 2). Samples are characterised by a porphyritic texture with average crystallinity and glassy groundmass fraction around 0.5. Ash particles from 17–18 November 2021, instead, are characterised by the presence of a few particles formed entirely by single crystals or only glass, while most of the particles are sideromelane (microlite poor glass) and tachylite (variably crystallised groundmass glass) (Figure 3). According to the componentry analysis (Section 2.4), the proportion of these different particles is ~1 % of single crystals, ~8 % of only glass, ~50 % of sideromelane, and ~40 % of tachylite (Supplementary Material 1 Figures S1–S2).

In all the analysed samples, we classified microlites those crystals under 0.03 mm [Zellmer 2021], while larger crystals are classified as microphenocrysts (between 0.03 and 0.2 mm) and phenocrysts (> 0.2 mm). The phase assemblage observed in both samples from 15 and 17–18 November comprises clinopyroxene and olivine phenocrysts and microphenocrysts, and glass, clinopyroxene, plagioclase and oxide in the groundmass. Particularly, clinopyroxene is the most abundant mineral phase (Φ_c = 0.1–0.3) and it is present as phenocrysts (0.2–0.6 mm), microphenocrysts (0.04–0.2 mm) and microlites (<0.02 mm). Phenocrysts display subhedral to euhedral shape, while both phenocrysts and microlites are characterised by concentric or patchy zoning with Al-rich cores, and occasionally by poikilitic textures with included Fe–Ti oxides (Figure 2). Olivine is present as subhedral phenocrysts and microphenocrysts (Φ_c = 0.1–0.15) ranging from 0.15 to 0.4 mm (Figure 2). Plagioclase (Φ_c = 0.02–0.08) is generally present as microlites that are tabular, acicular-tabular, or swallowtail (Figure 2). Finally, Fe–Ti oxides (Φ_c = 0.01–0.02) are usually subhedral-to-anhedral–shaped microlites and microphenocrysts up to 0.3 mm long.

3.2 Crystal phase composition and geothermobarometry

Samples from 15 November and 17–18 November display basanitic glass compositions with high alkali (~6–8 wt.% Na_2O + K_2O) and low silica contents (~43–46 wt.% SiO_2; Figure 4A and Supplementary Material 2 Table S4). These compositions fall in the range of compositions reported in previous studies for the 2021 eruption of Tajogaite on La Palma [Castro and Feisel 2022; Day et al. 2022; Pankhurst et al. 2022; Romero et

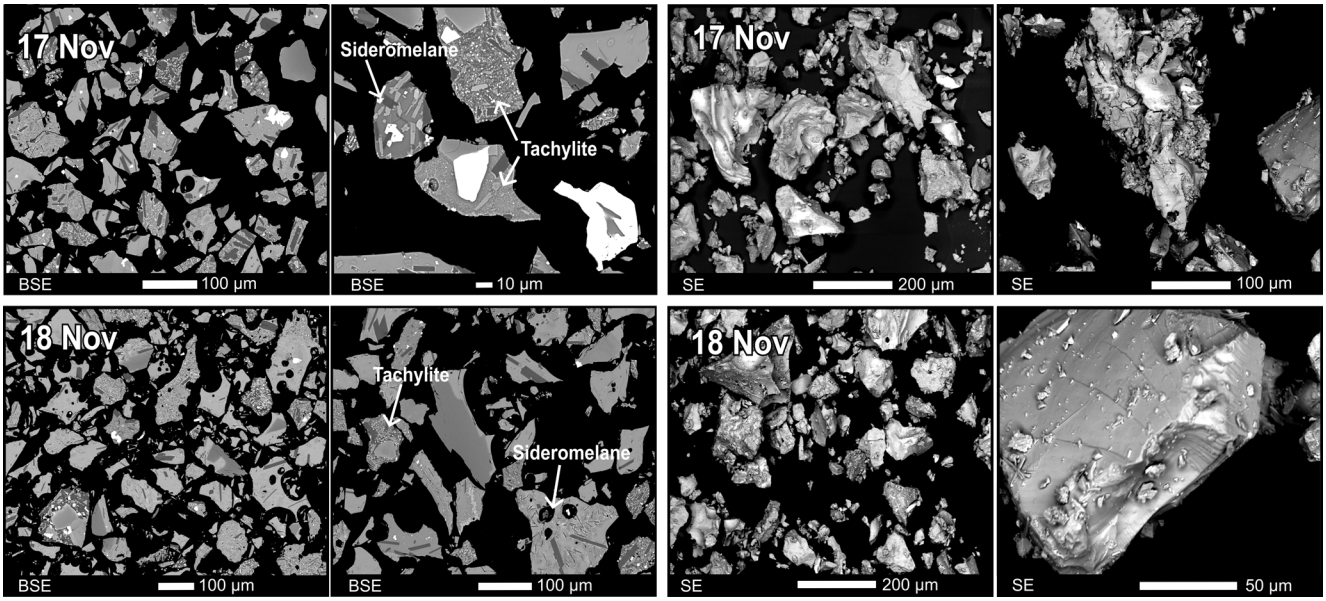

Figure 3: Backscattered electron images (BSE) and Secondary electron images (SE) of individual grains of ash samples from 17 and 18 November.

al. 2022; Dayton et al. 2023; Ubide et al. 2023]. In comparison with products of the previous Teneguía 1971 eruption [Barker et al. 2015], the 2021 eruption bulk-rock products reported in the literature so far are characterised by a comparatively more evolved composition (MgO between ~4 and 7 wt.%).

The dominant pyroxene composition in all samples is diopside ($Wo_{45–51}En_{34–43}Fs_{10–16}$; Figure 4B and Supplementary Material 2 Table S5), while plagioclase crystals are mostly labradorite ($An_{61–68}Ab_{30-37}Or_{1–3}$; Figure 4C and Supplementary Material 2 Table S6). Olivine crystals from 15 November samples have $Fo_{80–84}$ similar to the values reported by Dayton et al. [2023] for the same period, while olivine crystals from the 18 November sample have lower forsteritic content ($Fo_{74–80}$) (Supplementary Material 2 Table S7).

From clinopyroxene crystals and glass data we estimated the pre-eruptive temperatures and pressures using geothermobarometry (see Section 2.5 for details). All the obtained results are reported in Supplementary Material 2 Table S3, in Figure S3, and in Supplementary Data. For the H_2O-independent models we obtained T = 1135 ± 18 °C and P = 708 ± 99 MPa for MM_P03 and T = 1163 ± 7 °C and P = 792 ± 64 MPa for MM_P96. For the other models, instead, we observed that increasing water contents from 1 to 3 wt.% H_2O, we obtained decreasing temperatures and pressures as follows: from 1161 ± 12 to 1133 ± 12 °C and from 743 ± 160 to 691 ± 175 MPa for model MM_N17P08; from 1081 ± 14 to 1068 ± 12 °C and from 499 ± 82 to 517 ± 86 MPa for model MM_M13; from 1149 ± 14 to 1125 ± 19 °C and from 726 ± 67 to 708 ± 132 MPa for model MM_P03P08; and from 1158 ± 17 to 1133 ± 16 °C and from 740 ± 132 to 788 ± 145 MPa for model MM_P03P08. This test shows that the contribution of water content variations and the different P-T approaches are minor and within the calibration error of the thermobarometers. The only exception is the model of Masotta et al. [2013] whose P-T estimation are on average lower than those obtained with the other models. This is in agreement with the mismatch we observed between our data and their calibration dataset (calibrated for alkaline differentiated compositions such as trachytes and phonolites; Section 2.5 and Supplementary Material 1 Figure S4), suggesting in this case that P-T data may be underestimated. Overall, the obtained P-T estimates (Supplementary Material 1 Figure S3 and Table S3) are consistent with those reported by Castro and Feisel [2022] for samples from November, Romero et al. [2022] for samples from September–October, and González-García et al. [2023] and Ubide et al. [2023] for samples from September to December.

3.3 Textural analysis

Textural analysis was performed to quantify the area of crystal phases, matrix glass and vesicles in the 15 November samples. We focussed only on the samples from this day, because in samples of 17 and 18 November ash particles are too small to reliably segment mineral phases. In addition, we performed CSD analysis only on plagioclase crystals since clinopyroxene are too complexly zoned (see Figure 2) to obtained reliable residence time estimates. Indeed, CSD data are commonly used to infer crystal residence times, which require assumption of a single average growth rate for the entire phenocryst population [Cashman 2020]. Thus, applying CSD in presence of complex zoned phenocrysts and microphenocrysts may be misleading considering that (i) crystal cores do not always represent a single crystallisation event, and (ii) crystal rims form during magma ascent and thus represent the same crystallisation event responsible for nucleation and growth of groundmass crystals [Cashman 2020]. For this reason, large zoned crystals cannot be treated as a single crystallising population.

Obtained CSD plots (Figure 5) show a slight curvature for plagioclase, that may reveal pre-existing crystals growing as a separate population during magma ascent [e.g. Brugger and Hammer 2010; Cashman 2020], and/or nucleation of new mi-

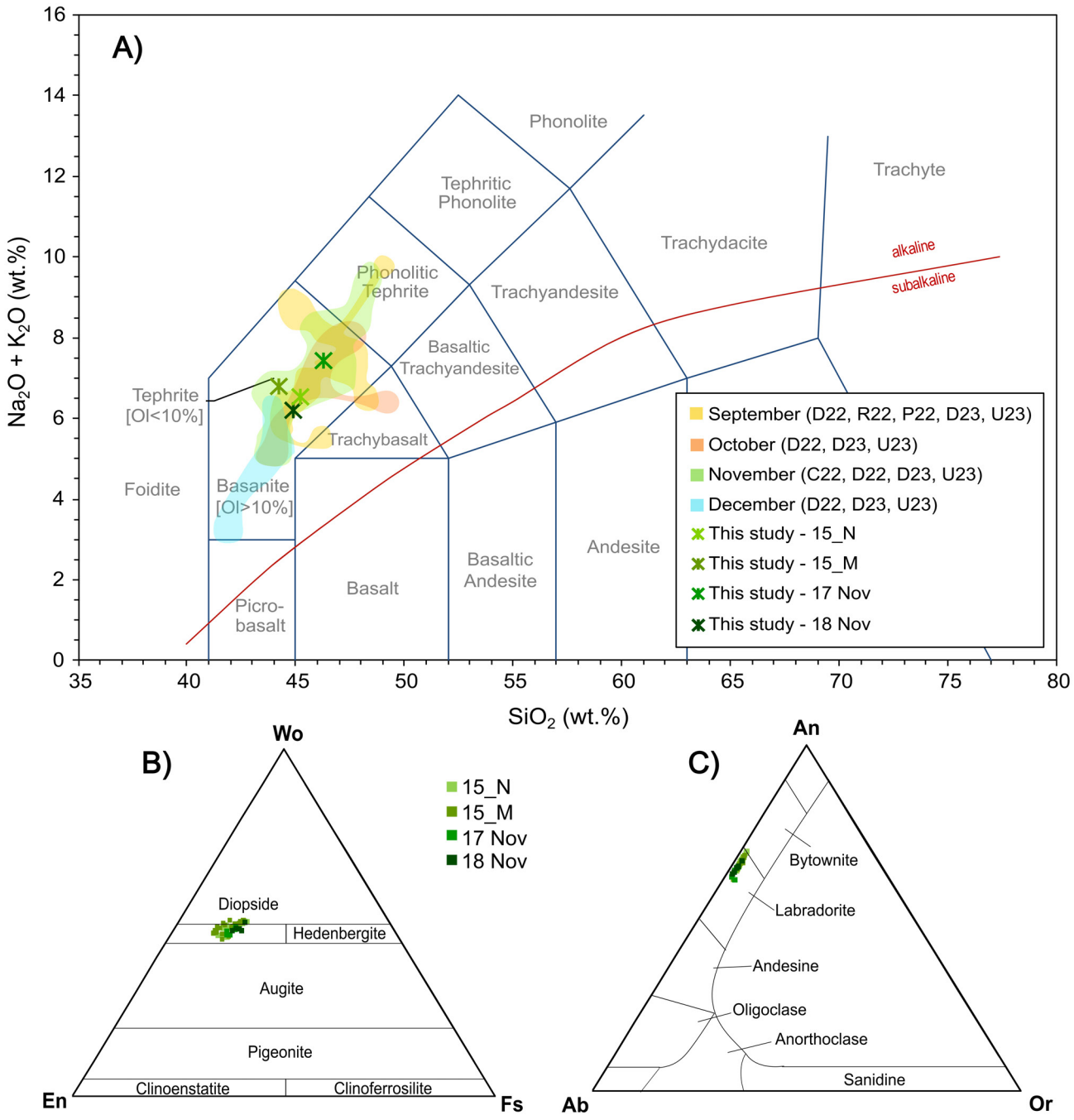

Figure 4: [A] TAS Diagram [Le Bas et al. 1986]. Coloured fields correspond to the 2021 Tajogaite glass compositions reported in literature (C22: Castro and Feisel [2022]; D22: Day et al. [2022]; P22: Pankhurst et al. [2022]; R22: Romero et al. [2022]; D23: Dayton et al. [2023]; U23: Ubide et al. [2023]). Error bars not shown since they are inside the symbols; [B]–[C] ternary classification diagrams for pyroxene and feldspar.

crolites at subsurface conditions [Thivet et al. 2020]. By using these plots, we estimated the crystallisation times (τ) of plagioclase crystal populations by using a range of experimentally derived growth rates (Gt) for basaltic melts [Shea and Hammer 2013; Arzilli et al. 2015; 2019; Bonechi et al. 2020] following the approach of Arzilli et al. [2016] and Bamber et al. [2020]:

$$\tau = \frac{-1}{Gt \cdot \text{slope}} \quad (1)$$

From 3D CSDs of plagioclase crystals we distinguish two populations of crystals (Figure 5 and Table 1), whose dimensions correspond to those initially determined as microlites and microphenocrysts (Section 3.1).

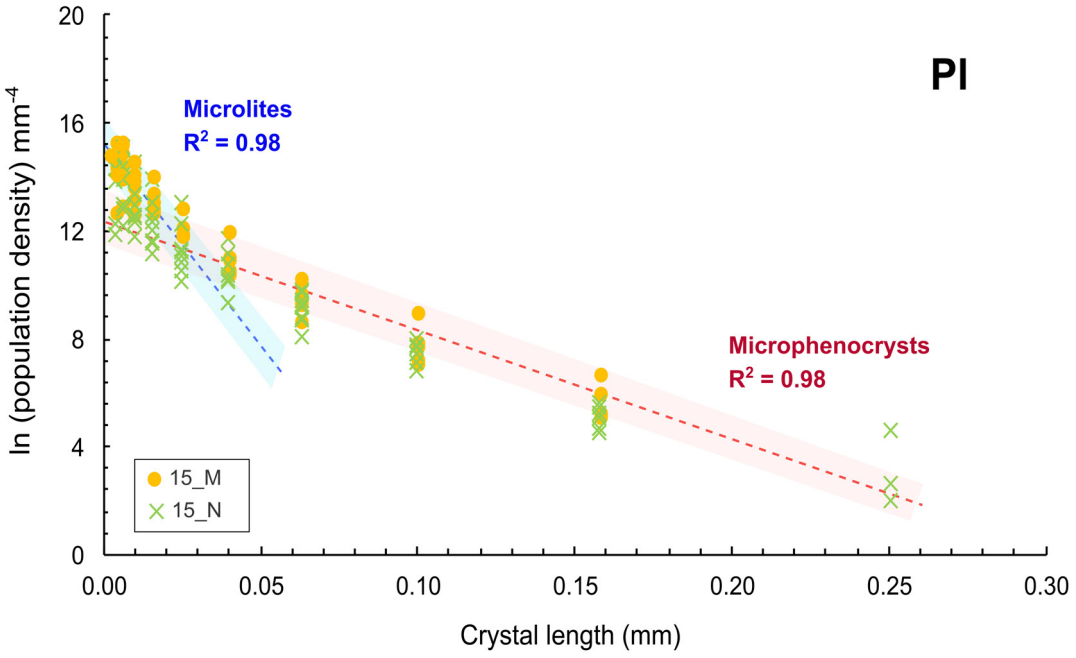

Figure 5: Crystal size distribution of the studied samples. Ln (population density) vs. crystal length (mm) plot for plagioclase samples from 15 November. For each identified crystal population linear regression (dashed lines: red for L > 0.03 mm, blue for L < 0.03 mm), standard deviation (coloured field: red for L > 0.03 mm, and blue for L < 0.03 mm) and correlation coefficient are reported. L refers to crystal length (mm).

Table 1: Summary of the average CSD analysis for selected samples, with geometric parameters (slopes and intercepts) of the straight-line regressions obtained from Figure 5. Note: σ is standard deviation. τ is crystallisation time obtained from Equation 1. Microlites (L < 0.03 mm), microphenocrysts (L > 0.03 mm). For plagioclase microphenocrysts and microlites we used growth rate of 1 × 10^{-6} mm s^{-1} after Shea and Hammer [2013], and 1 × 10^{-5} mm s^{-1} after Arzilli et al. [2015]. Data are from Pl crystals from 15 November 2021.

Size interval (mm)	Intercept (mm^{-4})	σ	Slope (mm^{-1})	σ	R^2	Growth rate (mm s^{-1})	τ (s)	σ	τ (min)	σ	τ (h)	σ
>0.03	12.4	1.0	−17.2	6.9	0.98	1 ×10^{-5} 1 ×10^{-6}	3392 33 917	1602 16 020	57 565	27 267	9	4
<0.03	14.9	0.9	−48.7	13.9	0.98	1 ×10^{-5}	1540	536	26	9		

4 Discussion

4.1 Evidence of a primitive melt composition feeding the second half of the eruption

La Palma eruption has been characterised by an increase of MgO content in the bulk rock composition from the beginning (September) to the end (December), with the least evolved composition (parental magma) recognised to have MgO = 8 wt.% [Day et al. 2022]. In addition to isotopic and seismic data supporting evidence of the arrival of a more primitive magma in the second half of the eruption [Day et al. 2022; Ubide et al. 2023], in this study, we provided further evidence of this conclusion by considering the geochemistry of plagioclase, which, being a late-stage phase, represents a particularly accurate proxy for the composition of erupting melt [Ubide et al. 2023]. We found that plagioclase microlites show a variation in some major oxides (i.e. Na_2O, K_2O and Al_2O_3) from September to November (Figure 6). Plagioclase compositions, indeed, are particularly sensitive to changes in temperature, H_2O pressure (pH_2O), and H_2O content [Cutler et al. 2022]. As shown in Figure 6, the first clear compositional difference through time is in the higher anorthite content ($An_{61–68}$) of the November plagioclase compared with that erupted in September ($An_{53–66}$); the more calcic plagioclases suggest relatively higher pH_2O and temperatures [Couch 2003; Cutler et al. 2022], as well as increasing melt maficity as observed also by Ubide et al. [2023]. Other differences observed are lower K_2O and Na_2O and higher Al_2O_3 contents in plagioclases from November compared with September. The November plagioclases have similar compositions to those of

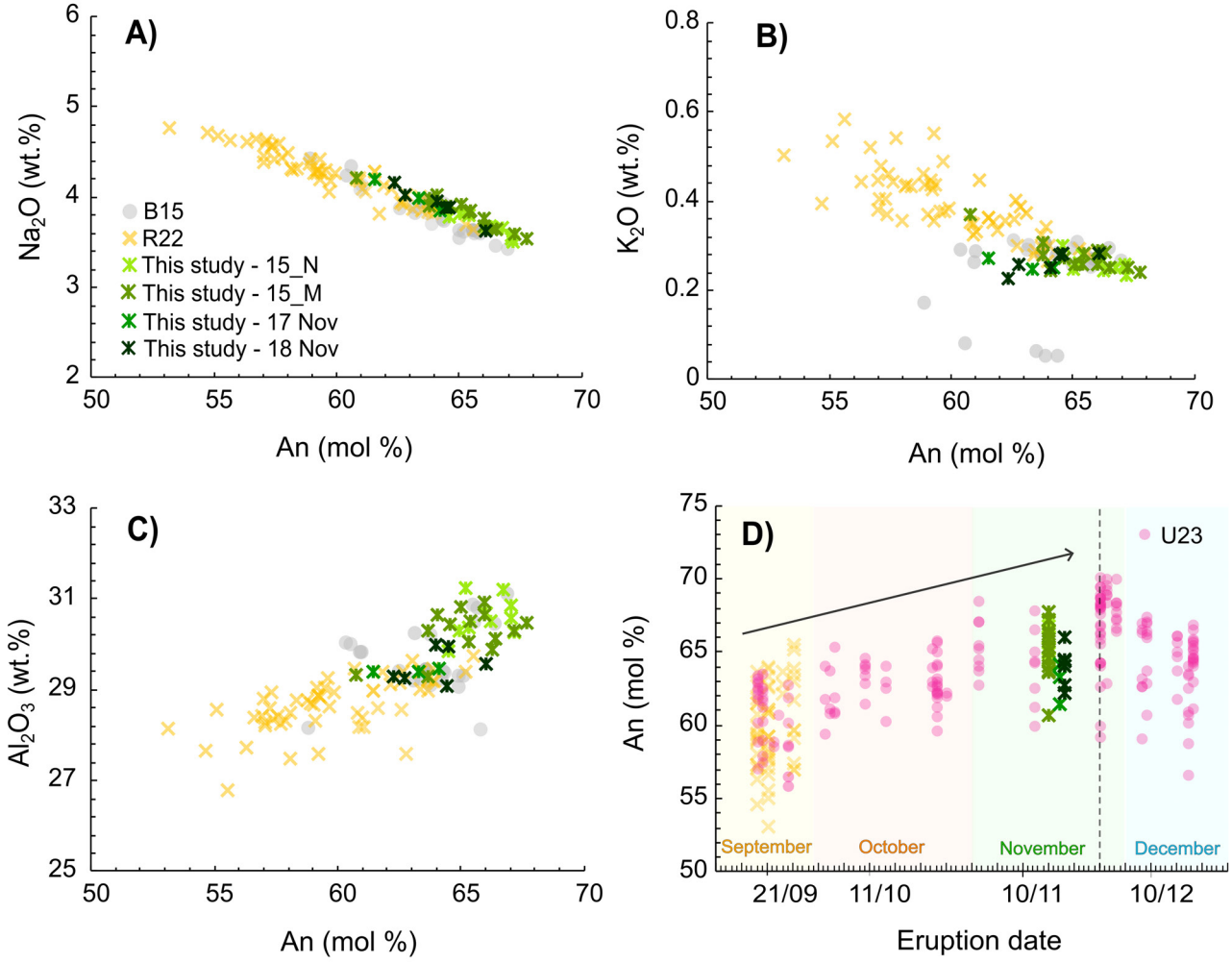

Figure 6: Na_2O [A], K_2O [B] and Al_2O_3 [C] vs An content for plagioclase of November (this study), September (R22 = Romero et al. [2022]) and previous Teneguía 1971 eruption (B15 = Barker et al. [2015]). [D] Temporal variation of An during the eruption (from September to December 2021) for plagioclase of this study, Romero et al. [2022] and Ubide et al. [2023]. As reported in Ubide et al. [2023] (U23), the geochemical kink on 25 November (dashed line) marks a turning point from recharge (before 25 November) to fractionation (after 25 November), indicating magma cooling and waning supply.

the Teneguía 1971 eruption available in Barker et al. [2015], as seen in Figure 6, suggesting that their formation occurred in presence of a more primitive melt composition with respect to that initially erupted in September.

4.2 Linking magma residence time, ascent rate and eruptive style of the November 2021 Tajogaite eruption

During magma ascent in the volcanic conduit, degassing, crystallisation processes and timescales play key roles in governing the evolution of magma geochemistry, eruption intensity and style, and ultimately the type and nature of the related geophysical signals [Pappalardo and Buono 2021]. In this light, we applied CSD data to gain information about pre-eruptive timescales and magma ascent velocities during its rise in the conduit (Figure 7). For plagioclase microphenocrysts of 15 November samples, considering experimental growth rates of 1×10^{-6} mm s^{-1} [Shea and Hammer 2013], we obtained a maximum crystallisation time (τ) of 9 ± 4 h (Table 1). The minimum residence time considering experimental growth rate of 1×10^{-5} mm s^{-1} [Arzilli et al. 2015] is 57 ± 27 minutes (Table 1). Conversely, the minimum residence time for microlites considering experimental growth rate of 1×10^{-5} mm s^{-1} [Arzilli et al. 2015] is 26 ± 9 minutes (Table 1).

In order to provide estimates on magma ascent rates we used the microlite number density exsolution rate meter of Toramaru et al. [2008]. Crystal area fraction (Φ_c) and area number density (N_A, mm^{-2}) on a vesicle-free basis were determined by thresholding, segmenting and counting crystals in each image. Number density and area fraction measurements were then used to calculate a mean crystal size, $S_N = (\Phi_c/N_A)^{1/2}$, and volumetric number density, $N_V = N_A/S_N$. The decompression rates [Cutler et al. 2022] at which microlites are formed are given by:

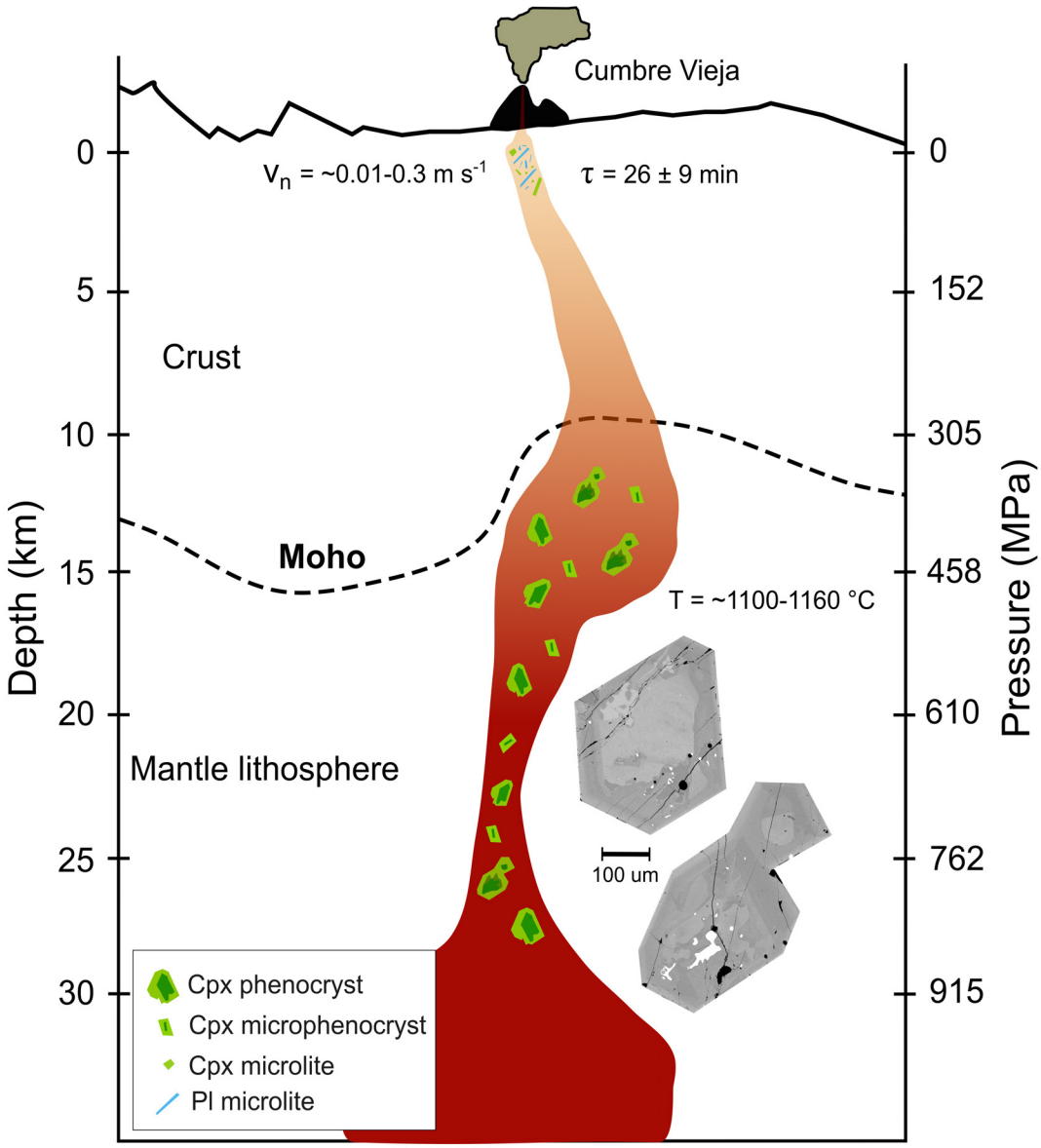

Figure 7: Schematic and simplified cartoon of the plumbing system during the 2021 La Palma eruption. Modified after D'Auria et al. [2022]. Particularly, we reported depths, temperatures (T) and times of crystallisation (τ) estimated through CSD and thermobarometry on samples of 15 November. We also reported magma ascent velocity (V_n) estimated by using the microlite number density exsolution rate meter of Toramaru et al. [2008] on plagioclase microlite population.

$$\left|\frac{dP_W}{dz}\right| = \frac{c}{b}\left(\frac{N_v}{a}\right)^{\frac{2}{3}}, \quad (2)$$

where P is pressure and z is depth, while c is a function of water content (C_W measured in wt.%) as: $c = 11.2 \times 10^6 \times C_W$, b is a constant (40 for plagioclase) and a depends on both C_W and the silica content (wt.%) $\Delta C_{Si} = C_{Si} - 50$ (wt.%) as: $a = 3 \times 10^{15\pm1+0.345\Delta C_{Si}-0.65C_W}$. For the calculation we selected a range of melt water contents from 1 to 3 wt.%, according to recent literature data on the 2021 La Palma eruption [Burton et al. 2023; Fabbrizio et al. 2023; Ubide et al. 2023].

Then, the magma ascent velocity (V_n [Cutler et al. 2022]) is calculated as:

$$V_n = \frac{1}{g \times \rho_v}\left|\frac{dP_W}{dz}\right|, \quad (3)$$

where ρ_v is the vesiculated magma density (obtained by using vesicle fraction values and a 2700 kg m^{-3} magma density) and g is the gravity acceleration.

The obtained ascent velocities range from 0.007 ± 0.004 (1 wt.% H_2O) to 0.15 ± 0.08 (3 wt.% H_2O) m s^{-1} for sample 15_N and from 0.013 ± 0.004 (1 wt.% H_2O) to 0.29 ± 0.09 (3 wt.% H_2O) m s^{-1} for sample 15_M (Table 2). These values are in agreement with those obtained through numerical modelling of magma ascent in volcanic conduit for the same period of eruptive activity [Biagioli et al. 2023]. The obtained values, moreover, fall within the area of sustained gas flows in eruptive conduits, thus with no significant inertial decoupling between gas and melt parts during magma ascent, favouring magma fragmentation at the subsurface, and ultimately leading to the formation of sustained lava fountains [e.g. Gonnermann and Manga 2013; Thivet et al. 2020]. They can also be associated with the formation of more or less ash-rich jets depending on the temperature, volatile, and viscosity evolution of the emitted magma within the lava fountain environment [e.g. Edwards et al. 2020; Namiki et al. 2021]. Finally, these values are comparable to those estimated by Romero et al. [2022] for samples from September (0.17–0.43 m s^{-1}) and they are coherent with the plagioclase microlites crystallisation time of 26 ± 9 minutes (Table 1), suggesting magma acceleration and fragmentation in the shallower part of the conduit [e.g. Cimarelli et al. 2010; Arzilli et al. 2019; Bamber et al. 2022].

Indeed, during 15 November, but also reported for other days of activity in the second half of the eruption, the occurrence of explosive activity characterized by the ejection of abundant dark ash and a strongly subordinate amount of visible lapilli and small bombs, with formation of low ($\lesssim$ 1–2 km), wind-bent plumes, was observed. This activity corresponds to the ash-rich jets reported in Taddeucci et al. [2023] and cannot be solely explained by considering the physicochemical characteristics of the November magma, which, besides the more primitive composition, are similar to those of the early phases of the eruption. We suggest that the triggering mechanisms of such explosive activity might be linked to a smaller conduit geometry, ejecta fallen back in the crater that created an obstruction, favouring gas entrapment and fragmentation, and/or lower gas emission rates. This interpretation can be supported also by the CSD analysis (i.e. slight curvature in the plagioclase plot) that can be related to nucleation of new microlites at subsurface conditions [Thivet et al. 2020]. This process, indeed, as observed in other mafic systems (e.g. Etna and Stromboli in Italy, and Gaua in Vanuatu) can lead to the formation of typical tachylite textures often linked with conduit narrowing/clogging (because of expected decreasing magma permeability and/or increasing magma viscosity and/or tephra recycling into the active vents), and finally enhance ash-rich explosive events [e.g. D'Oriano et al. 2014; Pompilio et al. 2017; Polacci et al. 2019]. Regarding gas emissions, instead, a strong decrease in SO_2 emission was observed from September (20–90 kt day^{-1}) to November (<10 kt day^{-1}; ~5 kt day^{-1} for 15 November) ([Ubide et al. 2023]; SO_2 daily emissions measured by TROPOMI*), which would suggest a decreased magma supply rate during the second half of the eruption. This may have created a reduced mass eruption rate and collapsing of the uppermost conduits, and promoted gas segregation into the explosive vents, with less gas entering the effusive vents, hence producing fragmentation in the explosive vent activity leading to the ash-rich jets of 15 November.

In agreement with previous works [e.g. Bonadonna et al. 2022; González-García et al. 2023; Taddeucci et al. 2023], the results of our study suggest that transitions in eruptive style during the Tajogaite eruption are likely the result of a complex feedback between several factors, including gas emission rate, fractionation of gas and magma between explosive and effusive vents, changes in conduit geometry, and magma ascent rates.

5 Conclusions

In this study the combination of compositional analyses, crystal size distribution data and geothermobarometry of tephra erupted during the November 2021 Tajogaite eruption (La Palma, Spain) allowed us to quantify magma storage depth, pre-eruptive conditions and magma ascent timescales in the second half of the eruption. In summary, we found that:

1. Geochemistry of plagioclase of the November products provided further evidence of the arrival of a more primitive magma. Plagioclase microlites show a variation in some major oxides from September to November (lower K_2O and Na_2O and higher Al_2O_3 contents in plagioclases from November) and a composition similar to that of plagioclases belonging to the Teneguía 1971 eruption, suggesting that their formation occurred in presence of a more primitive melt composition.

2. Crystal size distribution data and microlite number density provided information about pre-eruptive timescales and magma ascent velocities during its rise in the conduit. For plagioclase microlites from the 15 November samples minimum residence times are on the order of minutes (26 ± 9 minutes).

3. Obtained magma ascent velocities range from 0.007 ± 0.004 (1 wt.% H_2O) to 0.29 ± 0.09 (3 wt.% H_2O) m s^{-1} for 15 November samples. These values are comparable to those estimated for samples from September (0.17–0.43 m s^{-1}) and they are coherent with the plagioclase microlites crystallisation time of 26 ± 9 minutes, suggesting magma acceleration and fragmentation in the shallower part of the conduit.

4. The explosive activity characterizing the second half of the eruption and, in general, transitions in eruptive style throughout the Tajogaite eruption are likely the result of a complex interaction between gas emission rate, fractionation of gas and magma between explosive and effusive vents, changes in conduit geometry, and magma ascent rates.

Author Contributions

J.R. collected the volcanic rocks analysed in this study and provided background information about eruption activity observed during the field campaign of November 2021. B.B. and J.F. acquired back-scattered electron images of tephra samples. B.B performed image analysis, CSD calculations and geothermobarometry. B.B. assembled the manuscript and produced the figures with input from F.A., M.P. and J.R. All authors contributed to the discussion, data interpretation and editing of the manuscript.

*https://so2.gsfc.nasa.gov/

Acknowledgements

We warmly thank David Neave for fruitful discussions on this work, two anonymous reviewers whose comments allowed us to greatly improve the manuscript, and Alan Whittington for editorial handling. We are grateful to Instituto Volcanologico de Canarias (INVOLCAN), who allowed and supported our field activities during the crisis, and particularly Maria Asensio-Ramos and Nemesio M. Perez. Fieldwork was financed through NSFGEONERC-funded project DisEqm (NERC Reference: NE/N018575/1; NE/N018443/1) and V-PLUS projects. The research leading to these results has received funding from the UKRI FLF project 4DVOLC (MR/V023985/1). F. Arzilli thanks the KINETICVOLC project funded by the European Union, NextGenerationEU, Ministry of University and Research, Promotion and Development Fund DM737/2021.

Data Availability

Analytical data supporting the findings of this study are available within the article and its Supplementary Information. Supplementary Data for thermobarometry, error propagation, CSD, VND, and componentry analyses are available in the Zenodo archive (Version v1.3) at https://zenodo.org/doi/10.5281/zenodo.10044229 [Bonechi 2023].

References

Abràmoff, M. D., P. J. Magalhães, and S. J. Ram (2004). "Image processing with ImageJ". *Biophotonics international* 11(7), pages 36–42.

Arzilli, F., C. Agostini, P. Landi, A. Fortunati, L. Mancini, and M. R. Carroll (2015). "Plagioclase nucleation and growth kinetics in a hydrous basaltic melt by decompression experiments". *Contributions to Mineralogy and Petrology* 170(5–6). DOI: 10.1007/s00410-015-1205-9.

Arzilli, F., G. La Spina, M. R. Burton, M. Polacci, N. Le Gall, M. E. Hartley, D. Di Genova, B. Cai, N. T. Vo, E. C. Bamber, S. Nonni, R. Atwood, E. W. Llewellin, R. A. Brooker, H. M. Mader, and P. D. Lee (2019). "Magma fragmentation in highly explosive basaltic eruptions induced by rapid crystallization". *Nature Geoscience* 12(12), pages 1023–1028. DOI: 10.1038/s41561-019-0468-6.

Arzilli, F., M. Piochi, A. Mormone, C. Agostini, and M. R. Carroll (2016). "Constraining pre-eruptive magma conditions and unrest timescales during the Monte Nuovo eruption (1538 ad; Campi Flegrei, Southern Italy): integrating textural and CSD results from experimental and natural trachyphonolites". *Bulletin of Volcanology* 78(10). DOI: 10.1007/s00445-016-1062-z.

Table 2: Microlite crystal fraction (Φ_c), number density (N_A), mean crystal size (S_N), volumetric number density (N_V), nucleation depth (dP_w/dz, Equation 2), vesicle fraction (Φ_v), density of the bubbly magma ρ_v, and ascent velocities (V_n, Equation 3) for plagioclase crystal populations. Note: the density of the bubbly magma is obtained as: $\rho_v = \rho_m \times (1-\Phi_v)$, where ρ_m is the magma density (assumed to be 2700 kg m^{-3}) and Φ_v is the vesicle fraction measured from BSE images. Detailed error propagation is available as a Jupyter Notebook, archived via Zenodo[a] [Bonechi 2023].

Sample	Φ_c	σ	N_A (mm^{-2})	σ	S_N (mm)	σ	N_V (mm^{-3})	σ	C_{Si}	σ	ΔC_{Si}
15_N	0.06	0.01	281.04	190.04	1.43×10^{-2}	5.09×10^{-3}	1.97×10^{4}	1.51×10^{4}	45.2	0.23	−4.80
15_M	0.05	0.02	460.65	157.54	1.04×10^{-2}	2.38×10^{-3}	4.41×10^{4}	1.81×10^{4}	44.54	0.25	−5.46

Sample	C_w	c	b	a	σ	dP_w/dz	σ	Φ_v	ρ_v	V_n (m s^{-1})	σ
15_N	1	1.12×10^{7}	40	1.48×10^{14}	2.71×10^{13}	0.07	0.04	0.6	1080	0.007	0.004
	2	2.24×10^{7}	40	3.32×10^{13}	6.07×10^{12}	0.40	0.21	0.6	1080	0.04	0.02
	3	3.36×10^{7}	40	7.43×10^{12}	1.36×10^{12}	1.61	0.84	0.6	1080	0.15	0.08
15_M	1	1.12×10^{7}	40	8.78×10^{13}	1.74×10^{13}	0.18	0.05	0.5	1350	0.013	0.004
	2	2.24×10^{7}	40	1.97×10^{13}	3.90×10^{12}	0.96	0.29	0.5	1350	0.07	0.02
	3	3.36×10^{7}	40	4.40×10^{12}	8.74×10^{11}	3.91	1.19	0.5	1350	0.29	0.09

[a] https://zenodo.org/doi/10.5281/zenodo.10044229

Bamber, E. C., F. Arzilli, M. Polacci, M. E. Hartley, J. Fellowes, D. Di Genova, D. Chavarría, J. A. Saballos, and M. R. Burton (2020). "Pre- and syn-eruptive conditions of a basaltic Plinian eruption at Masaya Volcano, Nicaragua: The Masaya Triple Layer (2.1 ka)". *Journal of Volcanology and Geothermal Research* 392, page 106761. DOI: 10.1016/j.jvolgeores.2019.106761.

Bamber, E. C., G. La Spina, F. Arzilli, M. de'Michieli Vitturi, M. Polacci, M. E. Hartley, M. Petrelli, J. Fellowes, and M. Burton (2022). "Basaltic Plinian eruptions at Las Sierras-Masaya volcano driven by cool storage of crystal-rich magmas". *Communications Earth & Environment* 3(1). DOI: 10.1038/s43247-022-00585-5.

Barker, A. K., V. R. Troll, J. C. Carracedo, and P. A. Nicholls (2015). "The magma plumbing system for the 1971 Teneguía eruption on La Palma, Canary Islands". *Contributions to Mineralogy and Petrology* 170(5–6). DOI: 10.1007/s00410-015-1207-7.

Biagioli, E., G. La Spina, M. Polacci, J. E. Romero, B. Bonechi, M. Burton, and M. de'Michieli Vitturi (2023). "Numerical modelling integrated with field observations and analytical studies to assess eruptive style transitions at basaltic volcanoes". *IAVCEI Scientific Assembly, 30 Jan-3 Feb, Rotorua, New Zealand, Book of Abstracts*. Rotorua, New Zealand, page 96.

Blundy, J. and K. Cashman (2008). "Petrologic Reconstruction of Magmatic System Variables and Processes". *Reviews in Mineralogy and Geochemistry* 69(1), pages 179–239. DOI: 10.2138/rmg.2008.69.6.

Bonadonna, C., M. Pistolesi, S. Biass, M. Voloschina, J. Romero, D. Coppola, A. Folch, L. D'Auria, A. Martin-Lorenzo, L. Dominguez, C. Pastore, M.-P. Reyes Hardy, and F. Rodríguez (2022). "Physical Characterization of Long-Lasting Hybrid Eruptions: The 2021 Tajogaite Eruption of Cumbre Vieja (La Palma, Canary Islands)". *Journal of Geophysical Research: Solid Earth* 127(11). DOI: 10.1029/2022jb025302.

Bonechi, B. (2023). "Tajogaite-eruption—Volcanica-paper: v1.3". *Zenodo*. DOI: 10.5281/zenodo.10376756. [Dataset].

Bonechi, B., C. Perinelli, and M. Gaeta (2020). "Clinopyroxene growth rates at high pressure: constraints on magma recharge of the deep reservoir of the Campi Flegrei Volcanic District (south Italy)". *Bulletin of Volcanology* 82(1). DOI: 10.1007/s00445-019-1342-5.

Brugger, C. R. and J. E. Hammer (2010). "Crystal size distribution analysis of plagioclase in experimentally decompressed hydrous rhyodacite magma". *Earth and Planetary Science Letters* 300(3–4), pages 246–254. DOI: 10.1016/j.epsl.2010.09.046.

Burton, M., A. Aiuppa, P. Allard, M. Asensio-Ramos, A. P. Cofrades, A. La Spina, E. J. Nicholson, V. Zanon, J. Barrancos, M. Bitetto, M. Hartley, J. E. Romero, E. Waters, A. Stewart, P. A. Hernández, J. P. Lages, E. Padrón, K. Wood, B. Esse, C. Hayer, K. Cyrzan, E. F. Rose-Koga, F. Schiavi, L. D'Auria, and N. M. Pérez (2023). "Exceptional eruptive CO2 emissions from intra-plate alkaline magmatism in the Canary volcanic archipelago". *Communications Earth & Environment* 4(1). DOI: 10.1038/s43247-023-01103-x.

Carracedo, J. C., S. Day, H. Guillou, E. Rodríguez Badiola, J. A. Canas, and F. J. Pérez Torrado (1998). "Hotspot volcanism close to a passive continental margin: the Canary Islands". *Geological Magazine* 135(5), pages 591–604. DOI: 10.1017/s0016756898001447.

Carracedo, J. C., V. R. Troll, J. M. D. Day, H. Geiger, M. Aulinas, V. Soler, F. M. Deegan, F. J. Perez-Torrado, G. Gisbert, E. Gazel, A. Rodriguez-Gonzalez, and H. Albert (2022). "The 2021 eruption of the Cumbre Vieja volcanic ridge on La Palma, Canary Islands". *Geology Today* 38(3), pages 94–107. DOI: 10.1111/gto.12388.

Carracedo, J. C., E. R. Badiola, H. Guillou, J. de La Nuez, and F. J. P. Torrado (2001). "Geology and volcanology of la Palma and el Hierro, western Canaries". *Estudios Geologicos-Madrid* 57, pages 175–273.

Cashman, K. V. and S. M. McConnell (2005). "Multiple levels of magma storage during the 1980 summer eruptions of Mount St. Helens, WA". *Bulletin of Volcanology* 68(1), pages 57–75. DOI: 10.1007/s00445-005-0422-x.

Cashman, K. V. (2020). "Crystal Size Distribution (CSD) Analysis of Volcanic Samples: Advances and Challenges". *Frontiers in Earth Science* 8. DOI: 10.3389/feart.2020.00291.

Casillas Ruiz, R., J. d. l. Nuez Pestana, C. Fernández Rodrıguez, J. R. Colmenero, F. Jourdan, S. Harangi, R. Lukács, et al. (2020). "Edad de las rocas volcánicas submarinas y plutónicas del Complejo Basal de La Palma: implicaciones en la evolución geológica temprana de la isla". *Geogaceta* 67, pages 47–50.

Cassidy, M., M. Manga, K. Cashman, and O. Bachmann (2018). "Controls on explosive-effusive volcanic eruption styles". *Nature Communications* 9(1). DOI: 10.1038/s41467-018-05293-3.

Castro, J. M. and Y. Feisel (2022). "Eruption of ultralow-viscosity basanite magma at Cumbre Vieja, La Palma, Canary Islands". *Nature Communications* 13(1). DOI: 10.1038/s41467-022-30905-4.

Cimarelli, C., F. Di Traglia, and J. Taddeucci (2010). "Basaltic scoria textures from a zoned conduit as precursors to violent Strombolian activity". *Geology* 38(5), pages 439–442. DOI: 10.1130/g30720.1.

Couch, S. (2003). "The Kinetics of Degassing-Induced Crystallization at Soufriere Hills Volcano, Montserrat". *Journal of Petrology* 44(8), pages 1477–1502. DOI: 10.1093/petrology/44.8.1477.

Cutler, K. S., S. F. Watt, M. Cassidy, A. L. Madden-Nadeau, S. L. Engwell, M. Abdurrachman, M. E. Nurshal, D. R. Tappin, S. N. Carey, A. Novellino, C. Hayer, J. E. Hunt, S. J. Day, S. T. Grilli, I. A. Kurniawan, and N. Kartadinata (2022). "Downward-propagating eruption following vent unloading implies no direct magmatic trigger for the 2018 lateral collapse of Anak Krakatau". *Earth and Planetary Science Letters* 578, page 117332. DOI: 10.1016/j.epsl.2021.117332.

D'Auria, L., I. Koulakov, J. Prudencio, I. Cabrera-Pérez, J. M. Ibáñez, J. Barrancos, R. García-Hernández, D. Martínez van Dorth, G. D. Padilla, M. Przeor, V. Ortega, P. Hernández, and N. M. Peréz (2022). "Rapid magma ascent beneath La Palma revealed by seismic tomography". *Scientific Reports* 12(1). DOI: 10.1038/s41598-022-21818-9.

D'Oriano, C., A. Bertagnini, R. Cioni, and M. Pompilio (2014). "Identifying recycled ash in basaltic eruptions". *Scientific Reports* 4(1). DOI: 10.1038/srep05851.

Day, J. M., V. R. Troll, M. Aulinas, F. M. Deegan, H. Geiger, J. C. Carracedo, G. G. Pinto, and F. J. Perez-Torrado (2022). "Mantle source characteristics and magmatic processes during the 2021 La Palma eruption". *Earth and Planetary Science Letters* 597, page 117793. DOI: 10.1016/j.epsl.2022.117793.

Dayton, K., E. Gazel, P. Wieser, V. R. Troll, J. C. Carracedo, H. La Madrid, D. C. Roman, J. Ward, M. Aulinas, H. Geiger, F. M. Deegan, G. Gisbert, and F. J. Perez-Torrado (2023). "Deep magma storage during the 2021 La Palma eruption". *Science Advances* 9(6). DOI: 10.1126/sciadv.ade7641.

Edwards, M. J., L. Pioli, A. J. L. Harris, L. Gurioli, and S. Thivet (2020). "Magma fragmentation and particle size distributions in low intensity mafic explosions: the July/August 2015 Piton de la Fournaise eruption". *Scientific Reports* 10(1). DOI: 10.1038/s41598-020-69976-y.

Fabbrizio, A., E. C. Bamber, E. Michailidou, J. E. Romero, F. Arzilli, B. Bonechi, M. Polacci, and M. Burton (2023). "Phase equilibrium experiments and thermodynamic simulations to constrain the pre-eruptive conditions of the 2021 Tajogaite eruption (Cumbre Vieja volcano, La Palma, Canary Islands)". *Journal of Volcanology and Geothermal Research* 442, page 107901. DOI: 10.1016/j.jvolgeores.2023.107901.

Gonnermann, H. M. and M. Manga (2013). "Dynamics of magma ascent in the volcanic conduit". *Modeling Volcanic Processes*. Cambridge University Press, pages 55–84. DOI: 10.1017/cbo9781139021562.004.

González-García, D., T. Boulesteix, A. Klügel, and F. Holtz (2023). "Bubble-enhanced basanite–tephrite mixing in the early stages of the Cumbre Vieja 2021 eruption, La Palma, Canary Islands". *Scientific Reports* 13(1). DOI: 10.1038/s41598-023-41595-3.

Guillou, H., J. C. Carracedo, and S. J. Day (1998). "Dating of the Upper Pleistocene–Holocene volcanic activity of La Palma using the unspiked K–Ar technique". *Journal of Volcanology and Geothermal Research* 86(1–4), pages 137–149. DOI: 10.1016/s0377-0273(98)00074-2.

Gurioli, L., A. Di Muro, I. Vlastélic, S. Moune, S. Thivet, M. Valer, N. Villeneuve, G. Boudoire, A. Peltier, P. Bachèlery, V. Ferrazzini, N. Métrich, M. Benbakkar, N. Cluzel, C. Constantin, J.-L. Devidal, C. Fonquernie, and J.-M. Hénot (2018). "Integrating field, textural, and geochemical monitoring to track eruption triggers and dynamics: a case study from Piton de la Fournaise". *Solid Earth* 9(2), pages 431–455. DOI: 10.5194/se-9-431-2018.

Hammer, J. E., K. V. Cashman, R. P. Hoblitt, and S. Newman (1999). "Degassing and microlite crystallization during pre-climactic events of the 1991 eruption of Mt. Pinatubo, Philippines". *Bulletin of Volcanology* 60(5), pages 355–380. DOI: 10.1007/s004450050238.

Higgins, M. D. (2000). "Measurement of crystal size distributions". *American Mineralogist* 85(9), pages 1105–1116. DOI: 10.2138/am-2000-8-901.

Klügel, A., K. A. Hoernle, H.-U. Schmincke, and J. D. L. White (2000). "The chemically zoned 1949 eruption on La Palma (Canary Islands): Petrologic evolution and magma supply dynamics of a rift zone eruption". *Journal of Geophysical Research: Solid Earth* 105(B3), pages 5997–6016. DOI: 10.1029/1999jb900334.

Le Bas, M. J., R. W. Le Maitre, A. Streckeisen, and B. Zanettin (1986). "A Chemical Classification of Volcanic Rocks Based on the Total Alkali-Silica Diagram". *Journal of Petrology* 27(3), pages 745–750. DOI: 10.1093/petrology/27.3.745.

Longpré, M.-A. and A. Felpeto (2021). "Historical volcanism in the Canary Islands; part 1: A review of precursory and eruptive activity, eruption parameter estimates, and implications for hazard assessment". *Journal of Volcanology and Geothermal Research* 419, page 107363. DOI: 10.1016/j.jvolgeores.2021.107363.

Masotta, M., S. Mollo, C. Freda, M. Gaeta, and G. Moore (2013). "Clinopyroxene–liquid thermometers and barometers specific to alkaline differentiated magmas". *Contributions to Mineralogy and Petrology* 166(6), pages 1545–1561. DOI: 10.1007/s00410-013-0927-9.

Morgan, D. J. and D. A. Jerram (2006). "On estimating crystal shape for crystal size distribution analysis". *Journal of Volcanology and Geothermal Research* 154(1–2), pages 1–7. DOI: 10.1016/j.jvolgeores.2005.09.016.

Namiki, A., M. R. Patrick, M. Manga, and B. F. Houghton (2021). "Brittle fragmentation by rapid gas separation in a Hawaiian fountain". *Nature Geoscience* 14(4), pages 242–247. DOI: 10.1038/s41561-021-00709-0.

Neave, D. A., E. Bali, G. H. Guðfinnsson, S. A. Halldórsson, M. Kahl, A.-S. Schmidt, and F. Holtz (2019). "Clinopyroxene–Liquid Equilibria and Geothermobarometry in Natural and Experimental Tholeiites: the 2014–2015 Holuhraun Eruption, Iceland". *Journal of Petrology* 60(8), pages 1653–1680. DOI: 10.1093/petrology/egz042.

Neave, D. A. and K. D. Putirka (2017). "A new clinopyroxene-liquid barometer, and implications for magma storage pressures under Icelandic rift zones". *American Mineralogist* 102(4), pages 777–794. DOI: 10.2138/am-2017-5968.

Pankhurst, M. J., J. H. Scarrow, O. A. Barbee, J. Hickey, B. C. Coldwell, G. K. Rollinson, J. A. Rodríguez-Losada, A. Martín Lorenzo, F. Rodríguez, W. Hernández, D. Calvo Fernández, P. A. Hernández, and N. M. Pérez (2022). "Rapid response petrology for the opening eruptive phase of the 2021 Cumbre Vieja eruption, La Palma, Canary Islands". *Volcanica* 5(1), pages 1–10. DOI: 10.30909/vol.05.01.0110.

Pappalardo, L. and G. Buono (2021). *Insights Into Processes and Timescales of Magma Storage and Ascent From Textural and Geochemical Investigations: Case Studies From High-Risk Neapolitan Volcanoes (Italy)*. DOI: 10.1002/9781119564485.ch10.

Pappalardo, L., L. D'Auria, A. Cavallo, and S. Fiore (2014). "Petrological and seismic precursors of the paroxysmal phase of the last Vesuvius eruption on March 1944". *Scientific Reports* 4(1). DOI: 10.1038/srep06297.

Petrelli, M., L. Caricchi, and D. Perugini (2020). "Machine Learning Thermo-Barometry: Application to Clinopyroxene-Bearing Magmas". *Journal of Geophysical Research: Solid Earth* 125(9). DOI: 10.1029/2020jb020130.

Pioli, L., M. Pistolesi, and M. Rosi (2014). "Transient explosions at open-vent volcanoes: The case of Stromboli (Italy)". *Geology* 42(10), pages 863–866. DOI: 10.1130/g35844.1.

Polacci, M., D. Andronico, M. de'Michieli Vitturi, J. Taddeucci, and A. Cristaldi (2019). "Mechanisms of Ash Generation at Basaltic Volcanoes: The Case of Mount Etna, Italy". *Frontiers in Earth Science* 7. DOI: 10.3389/feart.2019.00193.

Polacci, M., R. A. Corsaro, and D. Andronico (2006). "Coupled textural and compositional characterization of basaltic scoria: Insights into the transition from Strombolian to fire fountain activity at Mount Etna, Italy". *Geology* 34(3), page 201. DOI: 10.1130/g22318.1.

Pompilio, M., A. Bertagnini, P. Del Carlo, and A. Di Roberto (2017). "Magma dynamics within a basaltic conduit revealed by textural and compositional features of erupted ash: the December 2015 Mt. Etna paroxysms". *Scientific Reports* 7(1). DOI: 10.1038/s41598-017-05065-x.

Preece, K., R. Gertisser, J. Barclay, S. J. Charbonnier, J.-C. Komorowski, and R. A. Herd (2016). "Transitions between explosive and effusive phases during the cataclysmic 2010 eruption of Merapi volcano, Java, Indonesia". *Bulletin of Volcanology* 78(8). DOI: 10.1007/s00445-016-1046-z.

Putirka, K., M. Johnson, R. Kinzler, J. Longhi, and D. Walker (1996). "Thermobarometry of mafic igneous rocks based on clinopyroxene-liquid equilibria, 0-30 kbar". *Contributions to Mineralogy and Petrology* 123(1), pages 92–108. DOI: 10.1007/s004100050145.

Putirka, K. D. (2008). "Thermometers and Barometers for Volcanic Systems". *Reviews in Mineralogy and Geochemistry* 69(1), pages 61–120. DOI: 10.2138/rmg.2008.69.3.

Putirka, K. D., H. Mikaelian, F. Ryerson, and H. Shaw (2003). "New clinopyroxene-liquid thermobarometers for mafic, evolved, and volatile-bearing lava compositions, with applications to lavas from Tibet and the Snake River Plain, Idaho". *American Mineralogist* 88(10), pages 1542–1554. DOI: 10.2138/am-2003-1017.

Ranero, C. R., M. Torne, and E. Banda (1995). "Gravity and multichannel seismic reflection constraints on the lithospheric structure of the Canary Swell". *Marine Geophysical Researches* 17(6), pages 519–534. DOI: 10.1007/bf01204342.

Roduit, N. (2007). "JMicroVision: versatile petrographic image analysis software". PhD thesis. University of Geneva.

Romero, J. E., M. Burton, F. Cáceres, J. Taddeucci, R. Civico, T. Ricci, M. J. Pankhurst, P. A. Hernández, C. Bonadonna, E. W. Llewellin, M. Pistolesi, M. Polacci, C. Solana, L. D'Auria, F. Arzilli, D. Andronico, F. Rodríguez, M. Asensio-Ramos, A. Martín-Lorenzo, C. Hayer, P. Scarlato, and N. M. Perez (2022). "The initial phase of the 2021 Cumbre Vieja ridge eruption (Canary Islands): Products and dynamics controlling edifice growth and collapse". *Journal of Volcanology and Geothermal Research* 431, page 107642. DOI: 10.1016/j.jvolgeores.2022.107642.

Ross, P.-S., T. Dürig, P. P. Comida, N. Lefebvre, J. D. L. White, D. Andronico, S. Thivet, J. Eychenne, and L. Gurioli (2022). "Standardized analysis of juvenile pyroclasts in comparative studies of primary magma fragmentation; 1. Overview and workflow". *Bulletin of Volcanology* 84(1). DOI: 10.1007/s00445-021-01516-6.

Saunders, K., J. Blundy, R. Dohmen, and K. Cashman (2012). "Linking Petrology and Seismology at an Active Volcano". *Science* 336(6084), pages 1023–1027. DOI: 10.1126/science.1220066.

Schneider, C. A., W. S. Rasband, and K. W. Eliceiri (2012). "NIH Image to ImageJ: 25 years of image analysis". *Nature Methods* 9(7), pages 671–675. DOI: 10.1038/nmeth.2089.

Scruggs, M. A. and K. D. Putirka (2018). "Eruption triggering by partial crystallization of mafic enclaves at Chaos Crags, Lassen Volcanic Center, California". *American Mineralogist* 103(10), pages 1575–1590. DOI: 10.2138/am-2018-6058.

Shea, T. and J. E. Hammer (2013). "Kinetics of cooling- and decompression-induced crystallization in hydrous mafic-intermediate magmas". *Journal of Volcanology and Geothermal Research* 260, pages 127–145. DOI: 10.1016/j.jvolgeores.2013.04.018.

Taddeucci, J., P. Scarlato, D. Andronico, T. Ricci, R. Civico, E. Del Bello, L. Spina, L. D'Auria, M. Asensio-Ramos, D. Calvo, E. Padrón, P. A. Hernández, and N. M. Pérez (2023). "The Explosive Activity of the 2021 Tajogaite Eruption (La Palma, Canary Islands, Spain)". *Geochemistry, Geophysics, Geosystems* 24(6). DOI: 10.1029/2023gc010946.

Tenzer, R., M. Bagherbandi, and P. Vajda (2013). "Global model of the upper mantle lateral density structure based on combining seismic and isostatic models". *Geosciences Journal* 17(1), pages 65–73. DOI: 10.1007/s12303-013-0009-z.

Thivet, S., L. Gurioli, and A. Di Muro (2020). "Basaltic dyke eruptions at Piton de La Fournaise: characterization of the eruptive products with implications for reservoir conditions, conduit processes and eruptive dynamics". *Contributions to Mineralogy and Petrology* 175(3). DOI: 10.1007/s00410-020-1664-5.

Toramaru, A., S. Noguchi, S. Oyoshihara, and A. Tsune (2008). "MND(microlite number density) water exsolution rate meter". *Journal of Volcanology and Geothermal Research* 175(1–2), pages 156–167. DOI: 10.1016/j.jvolgeores.2008.03.035.

Ubide, T., Á. Márquez, E. Ancochea, M. J. Huertas, R. Herrera, J. J. Coello-Bravo, D. Sanz-Mangas, J. Mulder, A. MacDonald, and I. Galindo (2023). "Discrete magma injections drive the 2021 La Palma eruption". *Science Advances* 9(27). DOI: 10.1126/sciadv.adg4813.

Wieser, P., M. Petrelli, J. Lubbers, E. Wieser, S. Ozaydin, A. Kent, and C. Till (2022). "Thermobar: An open-source Python3 tool for thermobarometry and hygrometry". *Volcanica* 5(2), pages 349–384. DOI: 10.30909/vol.05.02.349384.

Zellmer, G. F. (2021). "Gaining acuity on crystal terminology in volcanic rocks". *Bulletin of Volcanology* 83(11). DOI: 10.1007/s00445-021-01505-9.